Electronic Supporting Information for

Hysteretic spin crossover in iron(II) complexes of a new pyridine-triazole-pyrazine ligand is tuned by choice of NCE co-ligand

Ross W. Hogue, Reece G. Miller, Nicholas G. White, Humphrey L.C. Feltham, Guy N.L. Jameson, and Sally Brooker*

Department of Chemistry and MacDiarmid Institute for Advanced Materials and Nanotechnology, University of Otago, PO Box 56, Dunedin, 9054, New Zealand

Fax: +64 3 4797906

Tel: +64 3 4797919

E-mail: sbrooker@chemistry.otago.ac.nz

General remarks regarding synthesis

N-(4-methylphenyl)-2-pyridinecarbothioamide[S1] and pyrazine-2-carbohyrdazide[S2] were prepared as previously described. $[Fe(py)_4(NCS)_2]$, $[Fe(py)_4(NCSe)_2]$ and $[Fe(py)_4(NCBH_3)_2$ were prepared by mixing $FeCl_2$ and $NH_4(NCE)$ in water containing excess pyridine following the procedure described by Zuo and co-workers.[S3] Dry ethanol was prepared by distilling absolute ethanol from Mg/I_2. Other chemicals were bought commercially and used as received.

Synthesis of L^{pz}

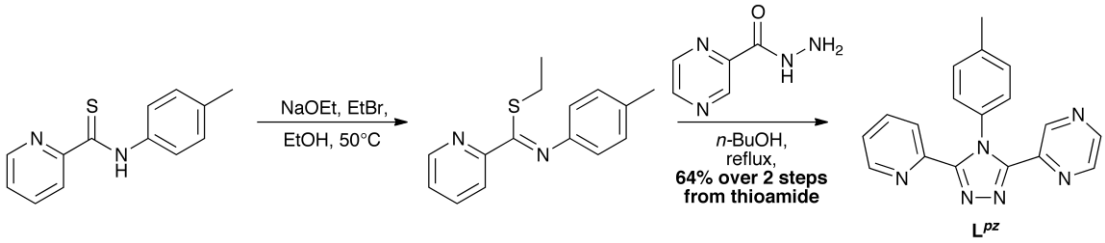

Scheme S1. Synthesis of $\mathbf{L}^{pz}$.

Sodium (0.069 g, 3.0 mmol) was dissolved in dry EtOH (12 mL), *N*-(4-methylphenyl)-2-pyridinecarbothioamide (0.631 g, 2.76 mmol) was added and the reaction stirred for 30 minutes to give an orange-brown solution. Bromoethane (0.346 g, 3.18 mmol) was added and the reaction stirred at 50 °C for 8 hours during which time a white precipitate formed. The suspension was left to stand at room temperature overnight then filtered, and the filtrate taken to dryness under reduced pressure. The resulting orange oil was taken up in CH_2Cl_2 (20 mL) and washed with water (3 × 5 mL), saturated $Na_2CO_{3(aq)}$ (5 mL), brine (5 mL) and dried ($MgSO_4$). It was taken to dryness under reduced pressure and then dissolved in *n*-BuOH (45 mL). Pyridine-2-carbohydrazide was added and the reaction mixture heated to reflux for 24 hours. Cooling the reaction mixture caused crystallization of $\mathbf{L}^{pz}$ as pale yellow crystals, which was isolated by filtration, washed with ethanol and dried thoroughly *in vacuo*. Yield: 0.456 g (56%). Evaporation of the filtrate and recrystallisation from isopropanol gave another 0.065 g (8%) of pure ligand. Combined yield: 0.521 g (64% over two steps from the thioamide).

^{1}H NMR (400 MHz, $CDCl_3$): 9.26 (s, 1H, 3-Pz*H*), 8.52 (d, ^3J = 2.0 Hz, 1H, 6-Pz*H*), 8.35–8.40 (m, 2H, 5-Pz*H*, 6-Py*H*), 8.06 (d, ^3J = 8.0 Hz, 1H, 3-Py*H*), 7.77 (app. t, ^3J ~ 7.7 Hz, 1H, 4-Py*H*), 7.24–7.27 (m, obscured by residual $CHCl_3$ peak, 5-Py*H*), 7.11–7.17 (m, 4H, Ph*H*), 2.39 (s, 3H, C*H*$_3$). ^{13}C NMR (100 MHz, $CDCl_3$): 155.0, 152.3, 149.2, 146.6, 145.3, 144.5, 143.5, 143.2, 138.9, 136.6, 133.0, 129.3, 127.6, 124.6, 124.1, 21.3. HRESI-MS (pos): 337.1171, calc. for $[C_{18}H_{14}N_6{\cdot}Na]^+$ = 337.1172. IR (ATR, *inter alia*): 3032, 1586, 1569, 1514, 1467, 1416, 1147, 1014, 823, 790, 707, 597 cm^{-1}. EA: C 68.6, H 4.5, N 26.9, calc. for $C_{18}H_{14}N_6$: C 68.8, H 4.5, N 26.7%. M.pt. 194 °C.

NMR spectra of L^{pz}

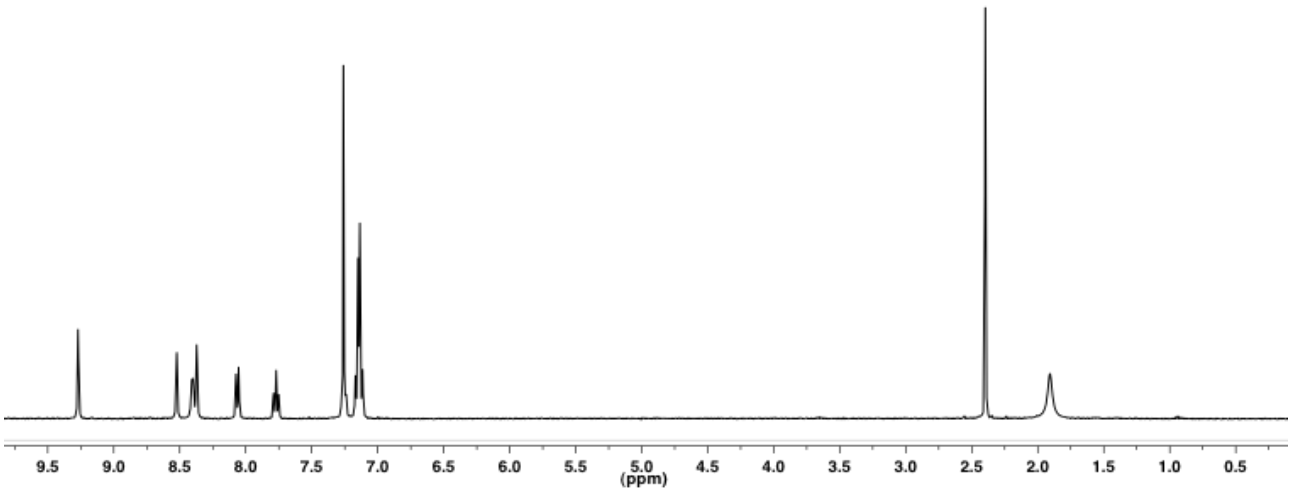

Figure S1. ^{1}H NMR spectrum of $\mathbf{L^{pz}}$ (400 MHz, $CDCl_3$, 298 K).

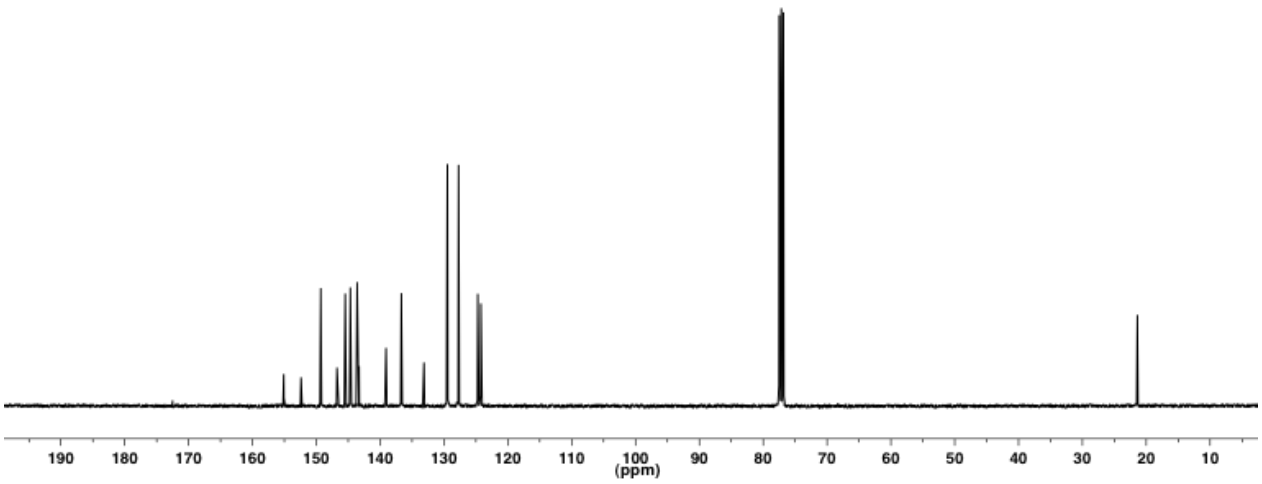

Figure S2. ^{13}C NMR spectrum of $\mathbf{L^{pz}}$ (100 MHz, $CDCl_3$, 298 K).

Complex synthesis

[Fe(L^{pz})$_2$(NCS)$_2$]

A pale yellow solution of **L^{pz}** (0.208 g, 0.664 mmol) in methanol (30 mL) was deoxygenated by bubbling Ar through it. A solution of [Fe(py)$_4$(NCS)$_2$] (0.161 g, 0.330 mmol) in methanol (10 mL) was similarly deoxygenated using Ar and then added to the ligand solution. The mixture was bubbled with Ar, then sealed and stirred for 24 h. During this time a dark red precipitate formed, and this was filtered under a stream of N_2 and dried *in vacuo* to give pure [Fe(**L^{pz}**)$_2$(NCS)$_2$]. Yield: 0.098 g (37%).

IR (ATR, *inter alia*): 2058, 1598, 1511, 1475, 1439, 1013, 826, 710, 608 cm^{-1}. HRESI-MS (pos.): 742.171, calc. for [Fe(**L^{pz}**)$_2$(NCS)]$^+$ = 742.166. EA: C 56.97, H 3.60, N 24.60; calc. for $C_{38}H_{28}N_{14}S_2Fe$: C 57.00, H 3.52, N 24.49%.

[Fe(L^{pz})$_2$(NCSe)$_2$]

A pale yellow solution of **L^{pz}** (0.130 g, 0.41 mmol) in methanol (20 mL) was deoxygenated by bubbling Ar through it. A solution of [Fe(py)$_4$(NCS)$_2$] (0.160 g, 0.28 mmol) in methanol (1 mL) added drop-wise to the ligand solution via a pipette loaded with celite (in order to remove traces of solid Se) eluting with methanol (4 mL). The mixture was bubbled with Ar, then sealed and stirred for 28 h. During this time a brick-red precipitate formed, and this was filtered under a stream of N_2 and dried *in vacuo* to give pure [Fe(**L^{pz}**)$_2$(NCSe)$_2$]. Yield: 0.095 g (52% based on **L^{pz}**). [Fe(L^{Pz})$_2$(NCSe)$_2$] was obtained in two polymorphs, a darker pink SCO active polymorph (**A**) and a pale pink HS polymorph (**B**). After multiple syntheses were carried out the majority of the time (>75%) polymorph **A** was obtained however no defining difference in the synthesis could be determined. IR (ATR, *inter alia*): 2063, 1599, 1511, 1476, 1440, 1014, 825, 711, 608 cm^{-1}. HRESI-MS (pos.): 790.108, calc. for [Fe(**L^{pz}**)$_2$(NCSe)]$^+$ = 790.110. EA: C 51.15, H 3.18, N 21.82, calc. for $C_{38}H_{28}N_{14}Se_2Fe$: C 51.02, H 3.16, N 21.92.

[Fe(L^{pz})$_2$(NCBH$_3$)$_2$]

[Fe(py)$_4$(NCBH$_3$)$_2$] (29.4mg, 65 µmol) was dissolved in isopropanol (25mL) and deoxygenated by bubbling with $N_{2(g)}$. A solution of **L^{pz}** (42.0mg, 134 µmol) in DCM (1mL) was deoxygenated in the same way and then added to the isopropanol solution. The resulting red suspension was sealed and stirred at ambient temperature for 18 hours. The resulting dark red solid was filtered under a flow of N_2(g) and washed with isopropanol (2 x 15mL), then Et_2O (2 x 15mL) and dried under a N_2(g) flow before further drying *in vacuo* to give pure [Fe(**L^{pz}**)$_2$(NCBH$_3$)$_2$]. Yield: 0.045 g (91%). IR (ATR, *inter alia*): 2323, 2164, 2075, 1512, 1444, 1016, 829, 708 cm^{-1}. HRESI-MS (pos.) 724.232, calc. for [Fe(**L^{pz}**)$_2$(NCBH$_3$)]$^+$ = 724.227. EA C 59.5, H 4.5, N 25.4; calc. for $FeC_{38}H_{34}B_2N_{14}$: C 59.7, H 4.5, N 25.7%.

Details of instrumentation and techniques

Elemental analyses were measured at the Campbell Micro-analytical Laboratory, University of Otago. IR spectra were recorded on a Bruker ATR-IR spectrometer with an Alpha-P module. ^{1}H and ^{13}C NMR spectra were recorded on a 400 MHz Varian 400MR spectrometer at 298 K. Chemical shifts are referenced to residual solvent peaks ($CDCl_3$: ^{1}H 7.26, ^{13}C 77.16 ppm). ESI mass spectra were recorded on a Bruker micrOTOFQ mass spectrometer in MeOH. Melting points were measured on a Mettler Toledo FP62 melting block.

^{57}Fe Mössbauer spectra were recorded on a Mössbauer spectrometer from SEE Co. equipped with a closed cycle refrigerator system from Janis Research Co. and SHI. Approximately 15–20 mg of sample was placed in a custom teflon sample holder (12.8 mm diameter, 0.5 mm thickness). Data were collected in constant acceleration mode in transmission geometry with an applied field of 47 mT parallel to the γ-rays. The zero velocity of the Mössbauer spectra refers to the centroid of the room temperature spectrum of a 25 μm metallic iron foil. Analysis of the spectra was conducted using the WMOSS program (SEE Co, formerly WEB Research Co. Edina, MN).

Magnetic data were recorded over the range 4–300 K using either a Quantum Design Physical Property Measurement System equipped with a vibrating sample mount (E = BH_3, Se), or a Quantum Design SQUID MPMS equipped with a reciprocating sample option (RSO) sample mount (E = S) using an applied field of 0.1 Tesla at Industrial Research Limited (now Callaghan Innovation), Lower Hutt, NZ. Data were corrected for the diamagnetism of the sample and a background correction for the sample holder was applied. The magnetic data over the range 50-300 K, collected at a sweep rate of 5 K min^{-1}, were corrected for temperature lag between the sample and instrument thermometer. This was done by measuring the temperature difference between the heating and cooling runs (outside of the range of the SCO event) that gave the same magnetic susceptibility, and assigning the mean temperature to this susceptibility whilst also noting the temperature correction. Doing this at several different places for each sample resulted in a constant temperature correction which was then applied across the 50-300 K range for that sample.

X-Ray crystallographic data for $\mathbf{L}^{pz}$ were collected on a Bruker Apex Kappa II area detector, using graphite-monochromated Mo-Kα radiation (λ = 0.710730(9) Å). The data were corrected for Lorentz and polarisation effects and semi-empirical absorptions corrections (SCALE) were applied.[S4] The structure was solved by direct methods (SHELXS-97) and refined against all F^2 data (SHELXL-97).[S5] All non-hydrogen atoms were refined anisotropically; hydrogen atoms were inserted at calculated positions and rode on the atoms to which they were attached with U(H) = 1.2U(non-H).

X-Ray crystallographic data for $[Fe(\mathbf{L}^{pz})_2(NCSe)_2]$ were collected using graphite monochromated Cu Kα radiation on an Oxford Diffraction SuperNova diffractometer equipped with a Cryostream N2 open-flow cooling device,[S6] at 100 and 260 K. Series of scans were performed in such a way as to collect a complete set of unique reflections to a maximum resolution of 0.80 Å. Raw frame data

(including data reduction, inter-frame scaling, unit cell refinement and absorption corrections) for all structures were processed using CrysAlis Pro.[S7] Structures were solved using SUPERFLIP[S8] and refined using full-matrix least-squares on F^2 within the CRYSTALS suite.[S9] All non-hydrogen atoms were refined with anisotropic displacement parameters. Hydrogen atoms were generally visible in the difference map and were initially refined with restraints on bond lengths and angles, after which the positions were used as the basis for a riding model.[S10] Crystallographic data for the structures have been deposited with the Cambridge Crystallographic Data Centre, CCDC: 937363-937365.

X-Ray powder diffraction patterns for [Fe($\mathbf{L}^{pz}$)$_2$(NCS)$_2$], [Fe($\mathbf{L}^{pz}$)$_2$(NCBH$_3$)$_2$] and polymorph **B** of [Fe($\mathbf{L}^{pz}$)$_2$(NCSe)$_2$] were collected in an aluminum sample holder (please note that peaks appearing at 2θ = 38.4 and 44.7 deg are an artifact of the aluminum sample holder) on a PANalytical X'Pert PRO MPD diffractometer at ambient temperature using Cu Kα radiation (λ = 1.54056 Å) over a 2 θ range from 3-50 degrees. Data was processed using PANalytical's X'Pert HighScore Plus (v2.2e). The PXRD pattern of SCO-active polymorph **A** of [Fe($\mathbf{L}^{pz}$)$_2$(NCSe)$_2$] was collected over a 2θ range from 6-50 degrees using graphite monochromated Cu Kα radiation on an Oxford Diffraction SuperNova diffractometer[S6] and the data processed using CrysAlis Pro.[S7]

Solid state structures of L^{pz} and $[Fe(L^{pz})_2(NCSe)_2]$ (polymorph B)

Table S1. Crystallographic data for $\mathbf{L^{pz}}$ and polymorph **B** of $[Fe(\mathbf{L^{pz}})_2(NCSe)_2]$.

	$\mathbf{L^{pz}}$	$[Fe(\mathbf{L^{pz}})_2(NCSe)_2]$ at 100 K	$[Fe(\mathbf{L^{pz}})_2(NCSe)_2]$ at 260 K
Empirical formula	$C_{18}H_{14}N_6$	$C_{19}H_{14}N_7SeFe_{0.5}$	$C_{19}H_{14}N_7SeFe_{0.5}$
Formula weight	314.35	447.26	447.26
Temperature (K)	93(2)	100(2)	260(1)
Wavelength	0.71073 Å	1.54184 Å	1.54184 Å
Crystal system	monoclinic	triclinic	triclinic
Space group	P2(1)/n	P-1	P-1
a (Å)	12.2509(13)	8.8651(2)	8.9760(3)
b (Å)	6.8857(9)	9.1919(2)	9.2721(6)
c (Å)	17.815(2)	11.5192(2)	11.5674(7)
α (°)	90	76.6530(17)	76.218(5)
β(°)	93.229(5)	77.0659(18)	77.043(4)
γ (°)	90	85.5043(17)	84.919(4)
Volume ($Å^3$)	1500.4(3)	889.78(3)	910.57(9)
Z	4	2	1
Density (calculated, in Mg/m^3)	1.392	1.669	1.631
Absorption coefficient (mm^{-1})	0.089	6.165	6.024
F(000)	656	448	448
Crystal size (mm^3)	0.70 x 0.15 x 0.09	0.22 x 0.14 x 0.08	0.22 x 0.14 x 0.08
Theta range for data collection (°)	3.17 to 26.38	4.04 to 76.56	4.025 to 76.531
Index ranges	-15<=h<=15 -8<=k<=8 -22<=l<=22	-11<=h<=9 -11<=k<=11 -14<=l<=14	-10<=h<=11 -11<=k<=11 -14<=l<=14
Reflections collected	19001	20539	7500
Independent reflections	3057 [R(int) = 0.0370]	3713 [R(int) = 0.0297]	3730 [R(int) = 0.0234]
Completeness to theta = 26.38° (%)	99.7	98.7	98.3
Absorption correction	Semi-empirical from equivalents	Semi-empirical from equivalents	Semi-empirical from equivalents
Max. and min. transmission	0.9920 and 0.9404	1.000 and 0.576	1.00 and 0.604
Refinement method	Full-matrix least-squares on F^2	Full-matrix least-squares on F^2	Full-matrix least-squares on F^2
Data / restraints / parameters	3057 / 0 / 218	3713 / 0 / 264	3715 / 0 / 250
Goodness-of-fit on F^2	1.054	1.194	0.9956
Final R indices [I>2sigma(I)]	R^1 = 0.0447, wR^2 = 0.1056	R^1 = 0.0297 wR^2 = 0.1227	R^1 = 0.0370 wR^2 = 0.0984
R indices (all data)	R^1 = 0.0546 wR^2 = 0.1117	R^1 = 0.0300 wR^2 = 0.1244	R^1 = 0.0389 wR^2 = 0.1012
Largest diff. peak and hole ($e.Å^{-3}$)	0.247 and -0.270	0.618 and -0.975	0.51 and -0.74

Figure S3. Solid state structure of $\mathbf{L}^{pz}$. Hydrogen atoms are omitted for clarity, thermal ellipsoids are drawn at 50% probability.

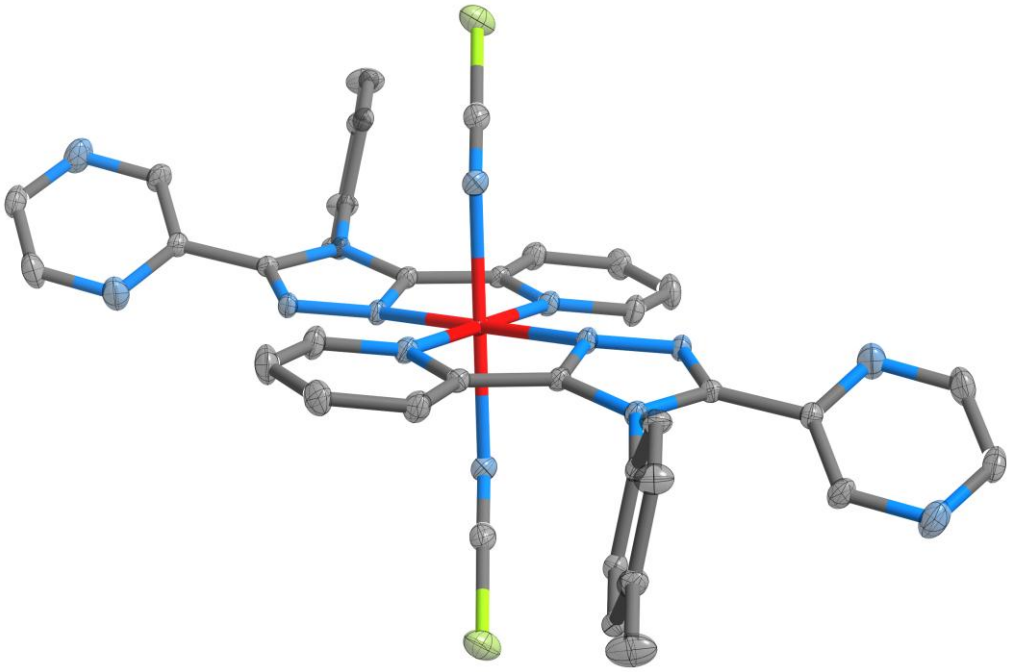

Figure S4. Solid state structure of polymorph **B** of $[Fe(\mathbf{L}^{pz})_2(NCSe)_2]$ at 100 K. Hydrogen atoms are omitted for clarity, thermal ellipsoids are drawn at 50% probability. The structure at 260 K is almost identical, and so is not shown.

The structures of $[Fe(\mathbf{L}^{pz})_2(NCSe)_2]$, polymorph **B**, at 100 and 260 K are almost identical (Figure S4). In both cases, the structures crystallize in the triclinic space group P-1, with half of the complex in the crystallographic asymmetric unit, and the iron centre located on the centre of inversion. As discussed in the text, Fe–N bond lengths and angles are consistent with a HS iron centre at both temperatures. The ligand coordinates in a bidentate manner through a pocket provided by *pyridine* and triazole nitrogen atoms, while the *pyrazine* heterocycle does not coordinate. The identity of the two 6-membered heterocycles (pyridine/pyrazine) was determined in several ways, all of which corroborate the proposed structure:

- The structure was modeled with all four possible identities of the rings (2 possible conformations of the non-coordinated pyrazine ring with coordinated pyridine; 2 possible conformations of the non-coordinated pyridine ring with coordinated pyrazine). The solution chosen gave the lowest R factors and most uniform U_{eq} values.

- All 12 atoms in the pyridine/pyrazine rings were manually changed to carbon, and the occupancies of these 12 atoms refined. Three refined to values significantly higher than one – these are the three nitrogen atoms in the proposed solution.

- Clear electron peaks corresponding to protons were visible in the difference map, approximately 1.0 Å from carbon atoms in the proposed structure. No peaks were visible near those atoms that we propose are nitrogen.

No significant hydrogen bonding or aromatic donor–acceptor interactions are observed in the structure, although a weak Se···Se contact is observed [Se···Se: 3.614(1) Å, 95% of the sum of van der Waal radii at 100 K; 3.657(1) Å, 96% of the sum of van der Waal radii at 260 K].

Powder X-ray diffraction patterns (PXRD) of iron(II) complexes

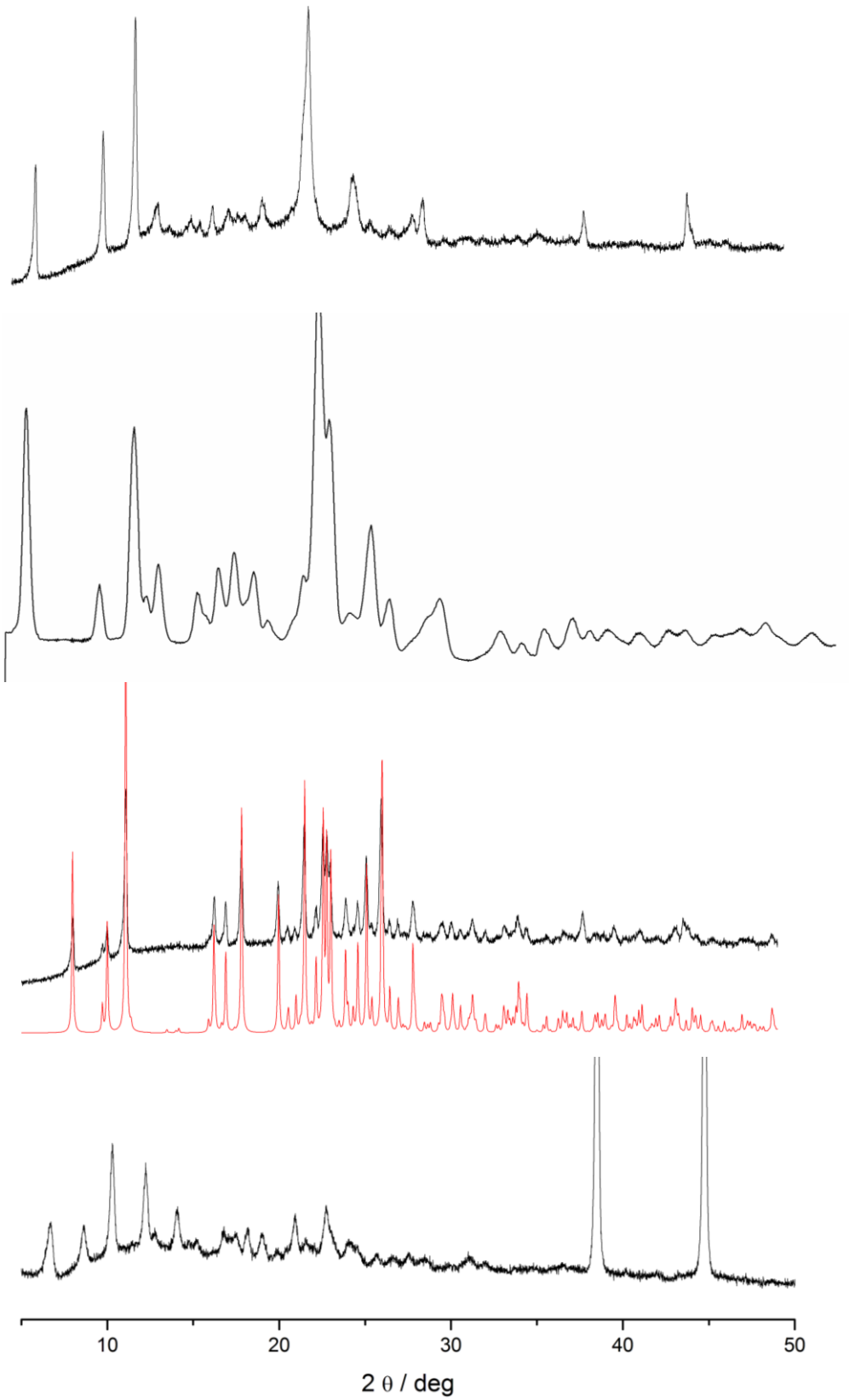

Figure S5. Top: Measured PXRD pattern for $[Fe(L^{Pz})_2(SCN)_2]$. Upper Middle: Measured PXRD pattern for SCO-active polymorph **A** of $[Fe(L^{Pz})_2(SeCN)_2]$. Lower Middle**:** Measured (black) and simulated (red) X-ray powder patterns for SCO-inactive polymorph **B** of $[Fe(L^{Pz})_2(SeCN)_2]$. Bottom: Measured PXRD patterns for $[Fe(L^{Pz})_2(BH_3CN)_2]$. The simulated powder pattern (red) was calculated based on the single crystal structure of SCO-inactive polymorph **B** of $[Fe(L^{Pz})_2(SeCN)_2]$. Please note that peaks appearing at 2θ = 38.4 and 44.7 deg are an artifact of the aluminum sample holder.

The powder diffraction patterns obtained for the SCO-active complexes [Fe($\mathbf{L}^{\mathbf{Pz}}$)$_2$(SCN)$_2$], [Fe($\mathbf{L}^{\mathbf{Pz}}$)$_2$(SeCN)$_2$] (polymorph **A**) and [Fe($\mathbf{L}^{\mathbf{Pz}}$)$_2$(BH$_3$CN)$_2$] (Figure S5) indicate these materials have some degree of crystallinity. All three have powder patterns that are very different to the predicted pattern (from the single crystal structure) of [Fe($\mathbf{L}^{\mathbf{Pz}}$)$_2$(SeCN)$_2$] (SCO-inactive polymorph **B**) so are not isostructural with it. A closer comparison of SCO-active [Fe($\mathbf{L}^{\mathbf{Pz}}$)$_2$(SCN)$_2$] and the SCO-active polymorph **A** of [Fe($\mathbf{L}^{\mathbf{Pz}}$)$_2$(SeCN)$_2$] (Figure S7) indicates some similarity in the solid state structure of these two compounds.

The PXRD pattern of a bulk powder sample of SCO-inactive polymorph **B** of [Fe($\mathbf{L}^{\mathbf{Pz}}$)$_2$(SeCN)$_2$] (Figures S5 and S6) shows a good match to the predicted pattern based on the single crystal structure of this compound at 260 K providing evidence that these materials are isostructural.

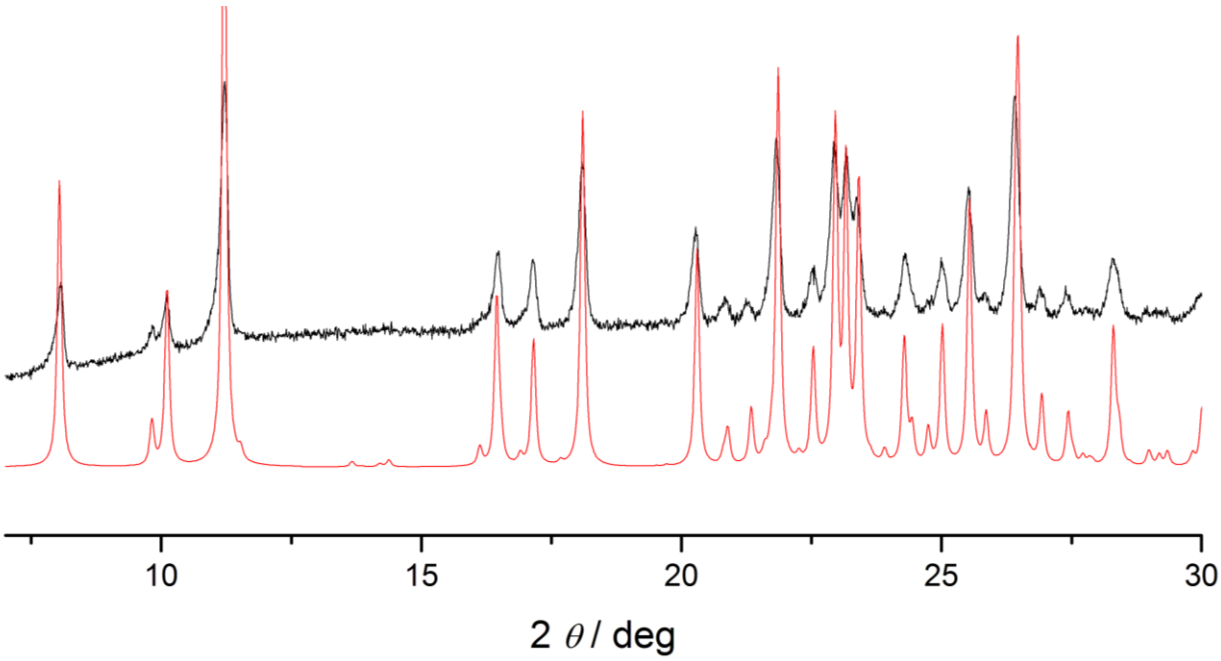

Figure S6 The observed vs calculated PXRD pattern, 2ϑ range from 7 – 30 degrees, for SCO-inactive **polymorph B** [Fe(L^{Pz})$_2$(SeCN)$_2$], enlarged for clarity. The simulated powder pattern was calculated based on the single crystal structure of [Fe(L^{Pz})$_2$(SeCN)$_2$] at 260 K.

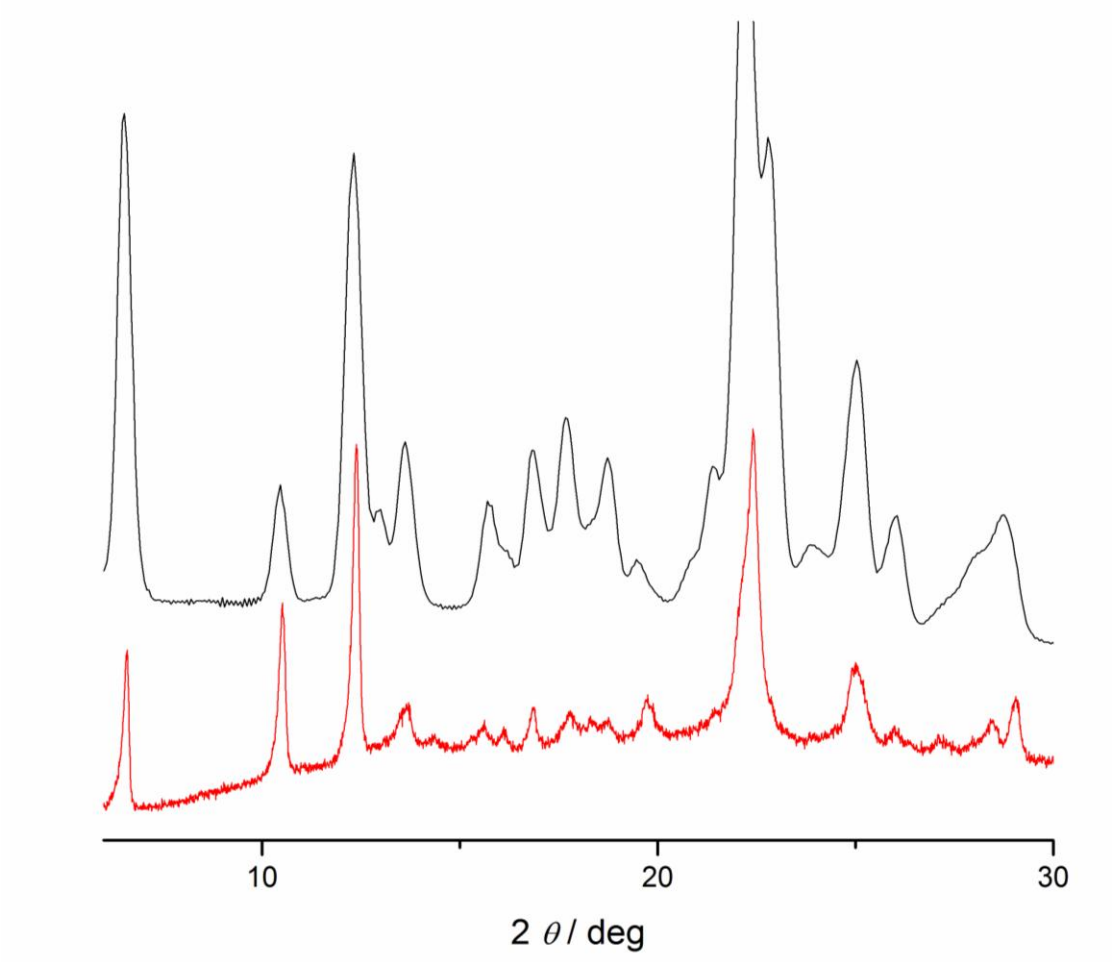

Figure S7. The PXRD patterns, measured at 298 K in the 2ϑ range from 6 – 30 degrees, of two of SCO-active complexes: polymorph **A** of $[Fe(L^{Pz})_2(SeCN)_2]$ (black) and $[Fe(L^{Pz})_2(SCN)_2]$ (red).

Additional magnetic data

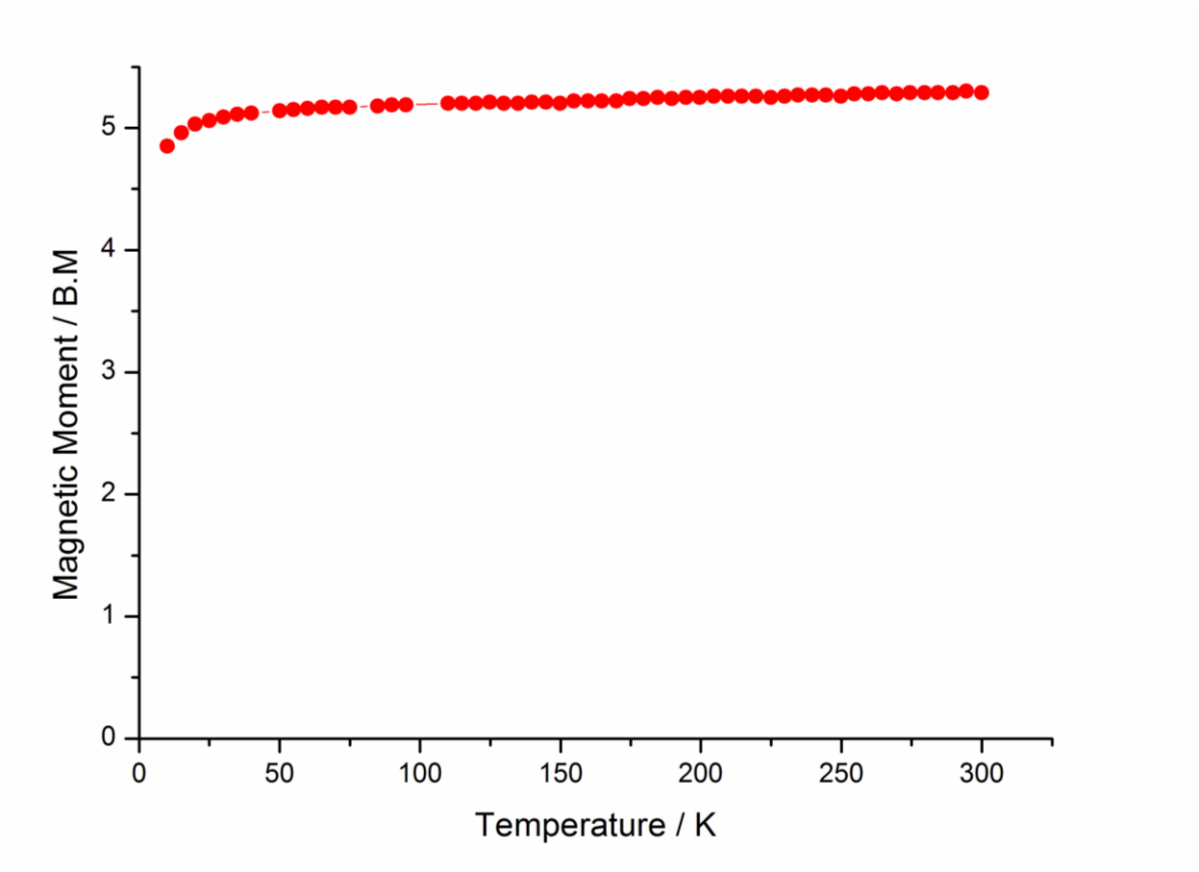

Figure S8. Magnetic moment as a function of temperature for the SCO inactive polymorph **B** of $[Fe(\mathbf{L}^{Pz})_2(SeCN)_2]$.

^{57}Fe Mössbauer spectroscopy

^{57}Fe Mössbauer spectra of [Fe($\mathbf{L}^{pz}$)$_2$(NCS)$_2$] were recorded at a variety of temperatures (Figure 4, Table S2): the sample was initially quench cooled in liquid nitrogen, before being cooled further in the spectrometer, to 5.3 K, before a spectrum was collected. It was then warmed slowly (~1 K/min), to 100 K, then 150 K and then 250 K, with spectra collected at each temperature. The sample was then slowly cooled back to 150 K and a spectrum collected. The spectral parameters are reported in Table S2.

Table S2. Mössbauer parameters for [Fe($\mathbf{L}^{pz}$)$_2$(NCS)$_2$] at the temperatures noted.

Temperature (K)	Species	δ (mm s^{-1})	ΔE_Q (mm s^{-1})	$\Gamma_{L=R}$ (mm s^{-1})	I (%)
5.3	HS	1.17	3.04	0.27	31 ± 2
	LS	0.52	0.44	0.24	69 ± 2
100	HS	1.15	3.05	0.28	31 ± 2
	LS	0.51	0.43	0.26	69 ± 2
150$_{warming}$	HS	1.12	3.09	0.26	54 ± 2
	LS	0.49	0.43	0.26	46 ± 2
250	HS	1.06	3.04	0.26	100
150$_{cooling}$	HS	1.12	3.09	0.26	83 ± 2
	LS	0.49	0.43	0.26	17 ± 2

The spectrum at 5.3 K comprises two sharp symmetrical quadrupole doublets, one with a large isomer shift and quadrupole splitting consistent with HS Fe(II), while the other has parameters are consistent with LS Fe(II). The relative intensities (I) of these signals indicates an approximate ratio of 3:7 HS:LS (Table S2). As the temperature increases, the intensity of the HS doublet increases and the intensity of the LS doublet decreases: at 250 K the compound is fully HS. Consistent with the magnetic data, these data indicate that an incomplete SCO, from fully HS to a mixture of HS and LS occurs. The difference in the two spectra collected at 150 K, one measured warming and the other cooling, confirmed that [Fe($\mathbf{L}^{pz}$)$_2$(NCS)$_2$] exhibits hysteretic SCO. At 150 K the HS fraction, γ_{HS} = 0.54 during warming, while during cooling γ_{HS} = 0.83.

The Mössbauer data for [Fe($\mathbf{L}^{pz}$)$_2$(NCSe)$_2$] show an almost complete SCO (Table S3, Figure S9), with a residual HS fraction of only γ_{HS} = 0.05 at 5.4 K, to a HS fraction of γ_{HS} = 0.85 at 250 K, consistent with most of the sample undergoing SCO. Consistent with the magnetic data, hysteresis is observed as different Mössbauer spectra are obtained at 170 K depending on whether the sample is being warmed or cooled. As with [Fe($\mathbf{L}^{pz}$)$_2$(NCS)$_2$], the Mössbauer spectra indicate that no oxidation to Fe(III) has occurred.

Table S3. Mössbauer parameters of [Fe($\mathbf{L}^{pz}$)$_2$(NCSe)$_2$] at the temperatures noted.

Temperature (K)	Species	δ (mm s^{-1})	ΔE_Q (mm s^{-1})	$\Gamma_{L=R}$ (mm s^{-1})	I (%)
5.4	HS	1.16	3.03	0.50	5 ± 2
	LS	0.51	0.43	0.24	95 ± 2
100	HS	1.18	3.06	0.50	10 ± 2
	LS	0.51	0.43	0.26	90 ± 2
170$_{warming}$	HS	1.09	3.17	0.28	20 ± 2
	LS	0.49	0.42	0.29	80 ± 2
250	HS	1.05	3.12	0.27	85 ± 2
	LS	0.26	0.30	0.50	15 ± 2
170$_{cooling}$	HS	1.10	3.18	0.27	29 ± 2
	LS	0.49	0.42	0.27	71 ± 2

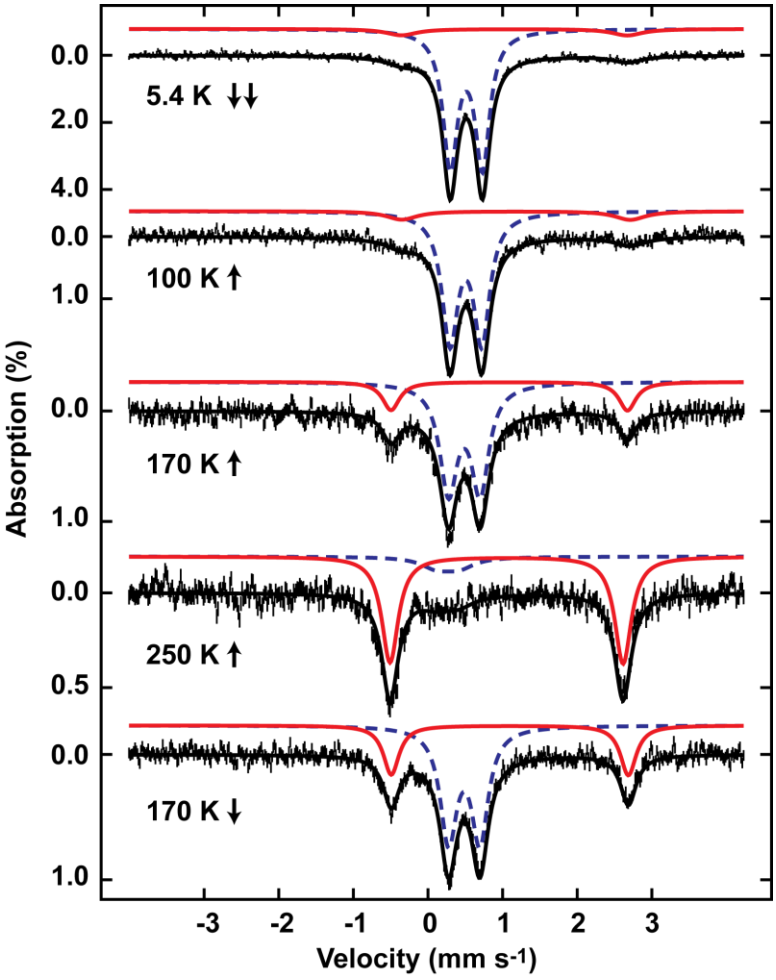

Figure S9. ^{57}Fe Mössbauer spectra of [Fe($\mathbf{L}^{pz}$)$_2$(NCSe)$_2$] measured at variable temperatures with an applied field of 47 mT parallel to the γ-rays. The sample was initially frozen rapidly in liquid nitrogen before being cooled to 5.4 K in the spectrometer. Slow warming (~1 K/min) to 100 K then 170 K and 250 K produced the spectra shown. The sample was then slowly cooled back to 170 K to show the presence of a hysteresis. The spectra are deconvoluted into high spin (red solid line) and low spin (blue dashed line) iron(II).

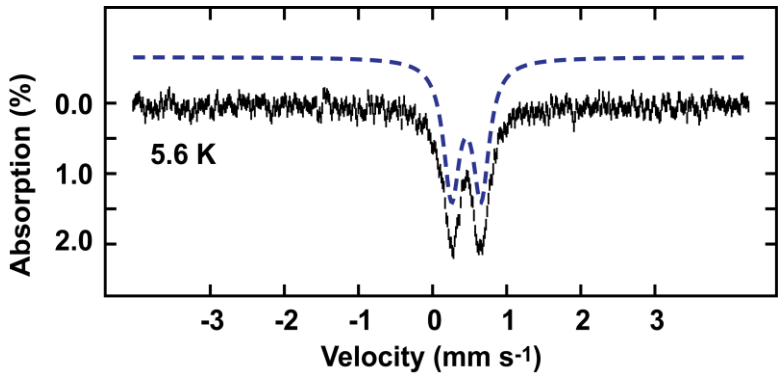

Figure S10. ^{57}Fe Mössbauer spectra of [Fe($\mathbf{L}^{pz}$)$_2$(H_3BCN)$_2$] measured at 5.6 K with an applied field of 47 mT parallel to the γ-rays. The spectrum can be fitted to a single symmetrical quadrupole doublet (blue dashed line) representing LS iron(II) with parameters δ = 0.46 mm s^{-1}, ΔE_Q = 0.40 mm s^{-1}, $\Gamma_{L=R}$ = 0.26 mm s^{-1}.

References

S1 M.H. Klingele, S. Brooker, *Eur. J. Org. Chem.*, **2004**, 3422.

S2 F.M.F. Vergara, C.H. da S. Lima, M das Graças, M. de O. Henriques, A.L.P. Candéa, M.C.S. Lourenço, M. de L. Ferreira, C.R. Kaiser, M.V.N. de Souza, *Eur. J. Med. Chem.*, **2009**, 44, 4954.

S3 J-Q. Tao, Z-G. Gu, T-W. Wang, Q-F. Yang, J-L. Zuo, X-Z. You, *Inorg. Chim. Acta*, **2007**, 360, 4125.

S4 G.M. Sheldrick, *SADABS: Empirical absorption correction program for area detector data*, Göttingen, **1996**.

S5 G.M. Sheldrick, *Acta Crystallogr.*, **2008**, A64, 112.

S6 J. Cosier, A.M. Glazer, *J. Appl. Crystallogr.*, **1986**, 19, 105.

S7 CryAlisPRO, *Oxford Diffraction*, **2011**.

S8 L. Palatinus, G. Chapuis, *J. Appl. Crystallogr.*, **2007**, 40, 786.

S9 P.W. Betteridge, J.R. Carruthers, R.I. Cooper, K. Prout, D.J. Watkin, **2003**, *J. Appl. Crystallogr.*, 36, 1487.

S10 R.I. Copper, A.L. Thompson, D.J. Watkin, *J. Appl. Crystallogr.*, **2010**, 43, 1100.